MATHEMATICAL AND TECHNOLOGICAL APROACH OF ON-CHIP INTERCONECT CONCAVE MICROMIRROR

Roxana-Mariana BEIU[1], C-tin. D. STĂNESCU[2]

Tendinţa de miniaturizare continuă conduce la noi abordări teoretice şi aplicaţii în domeniile electronicii, opticii, şi mecanicii. Domeniul vast al microoptoelectronicii este în continuă expansiune datorită multiplelor avantaje oferite de utilizarea luminii ca purtătoare de informaţie (fără perturbări în câmp electric şi/sau magnetic). În consecinţă, a apărut inevitabilă o nouă abordare a opticii la dimensiuni de ordinul micrometrilor.

Lucrarea are ca punct de plecare un modul optoelectronic CMOS, propus de E. Fullin ş.a., şi detaliază atât matematic cât şi tehnologic, modalitatea de realizare a unei microoglinzi concave optimale, utilizată la conexiunile din interiorul circuitelor integrate (prin intermediul fibrelor optice).

The enduring trend towards miniaturization leads to new theoretical approaches and applications for the electronics, optics, and fine mechanics domains. The expansion of microoptoelectronics is continuous due to the countless advantages of using light in communications (i.e., without electric and/or magnetic field perturbations). Consequently, new approaches for taking advantage of optics at the micrometer range are currently being developed.

The paper starts from an integrated optoelectronics approach for CMOS-based technology which was proposed by Fullin et al. and details a theoretical and technological approach for the design of an optimal concave micromirror, to be used for on-chip communications (in conjunction with fiber optics).

Keywords: micromirror, MOEMS, gray-tone mask, on-chip connection.

1. Introduction

There is a growing trend towards miniaturization and integration of components and systems in many fields of engineering, in order to significantly reduce their *size*, *weight*, *power consumption* and *cost*. This trend is particularly apparent in optics, where recent years have witnessed a rapid growth in such (new or renewed) fields as: micro-optics, integrated optics and micro-opto-electro-mechanical systems (MOEMS) [1].

[1] Eng., PhD student, University POLITEHNICA of Bucharest, Romania,
[2] Prof. Dept. of Engineering and Management of Technological Systems, University POLITEHNICA of Bucharest, Romania

Integrated devices based on MOEMS can lead to free-space integrated optics and are consequently pushing towards the development of optical on-chip interconnect [2, 3].

Fullin *et al.* [4] have proposed as early as 1994 a possible interconnect method to be used (see also [5]) inside a chip. The idea (see Fig. 1) is quite simple and interesting: "*the coupling between the waveguide and the electronics consists of a tapered waveguide end, acting as a mirror, which deflects the guided light towards an integrated photodiode [...]. Compared to other coupling structures this tapered end has the main advantage of keeping the waveguide structures perfectly flat in the photodiode region.*"

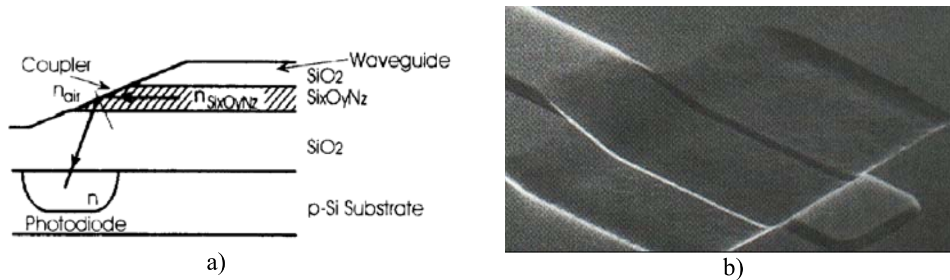

Fig. 1. Basic idea from Fullin *et al.* [4]: a) Schematic view; b) Scanning electron microscopy of a waveguide.

In this paper we use the same approach. The main goal of this paper is to show how the optical signal could be enhanced. For a better response of the integrated photodiode, we need to preserve the light intensity by using a coated curved micromirror instead of a n_{air}–$n_{SixOyNz}$ coupler.

As can be seen from Fig. 2, the light wave coming through the optical fiber will be focused in the focal plane of the curved mirror. This will enhance the overall response of the optical system.

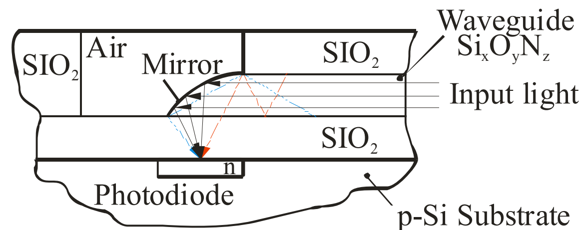

Fig. 2. Optical on-chip interconnection scheme using curved micromirror, and optical fiber.

An estimate can be made starting from a larger dimensional scale. Instead of the 3.5 μm × 0.35 μm [4] dimensions for fiber optic we shall start with a semispherical one (r = 6 μm) and use only the upper part with height of $r/2$. We will then show how to optimize the dimensions (*i.e.*, reduce them) and the shape of the mirror, relatively to technological conditions and light propagation.

2. Spherical mirror

A spherical mirror is a mirror, which has the shape of a piece cut out of a spherical surface. The most commonly occurring examples of concave mirrors are shaving mirrors and makeup mirrors. As it is well known, these types of mirrors magnify objects placed close to them. Concave mirrors have wider fields of view than equivalent flat mirrors, but objects seen through them, generally look smaller (and, therefore, farther away) than they actually are.

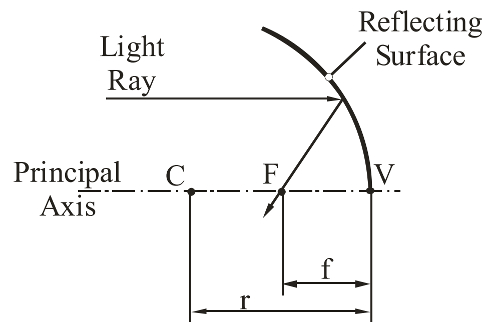

Fig. 3. The elements of a concave mirror: the vertex (V), the center (C), and the focal point (F).

The normal to the center of the mirror is called the principal axis (see Fig. 3). The mirror is assumed to be rotationally symmetric about its principal axis. This allows to represent a three dimensional mirror in a two dimensional diagram without loss of generality.

The point V at which the principal axis touches the surface of the mirror is called the vertex. The point C, on the principal axis, which is equidistant from all points on the reflecting surface of the mirror, is called the center of curvature. The distance along the principal axis from point C to point V is called the radius of curvature of the mirror, and is denoted by r.

A concave mirror receiving input rays to its principal axis, and *not too far away from this axis*, will focus them through the same point on the principal axis. This point, which lies between the center of curvature C and the vertex V, is called the focal point F, or focus of the mirror. The distance along the principal

axis from the focus F to the vertex V is called the focal length of the mirror, and is denoted by f.

In general one assumes that all light-rays which arrive at a mirror, parallel to its principal axis (*e.g.*, all rays emanating from a distant object) are brought to focus at the same point F. Of course, as mentioned above, this is only an approximation. The lack of perfect focusing of a spherical mirror is called spherical aberration. Neglecting the spherical aberration is an approximation known as the paraxial approximation.

From the equation of a spherical mirror:

$$\frac{2}{R} = \frac{1}{p} + \frac{1}{q} \tag{1}$$

(where p and q are the distances from object and image to the mirror surface) we can compute f. As can be seen from Fig. 3, f is the focal distance corresponding to a ray coming from very far away (infinity), so $p = \infty$ leading to $f = R/2$.

3. Parabolic mirror

It can be proven geometrically that the only type of mirror, which does not suffer from spherical aberration, is a parabolic mirror (*i.e.*, a mirror whose reflecting surface is the surface of revolution of a parabola). Thus, a ray traveling parallel to the principal axis of a parabolic mirror is brought to a focus at the same point F, no matter how far the ray is from the axis. Since the path of a light-ray is perfectly reversible, it follows that a light source placed at the focus F of a parabolic mirror yields a parallel beam of light, after the light is reflected off the surface of the mirror. This characteristic also explains why this type of mirror is used for satellite dishes as well as for automobile headlights.

From the equation of a circle, of radius r in Cartesian coordinates:

$$y^2 + (x-r)^2 = r^2 \text{, or } y^2 - 2xr + x^2 = 0 \tag{2}$$

we obtain one solution for $x \le r$:

$$x = r - \sqrt{r^2 - y^2} \tag{3}$$

Expanding the square root of equ. (3) in a binomial series gives:

$$x = \frac{y^2}{2r} + \frac{y^4}{2^3 r^3} + \frac{y^6}{2^4 r^5} + \ldots \tag{4}$$

Equation (4) corresponds to a spherical mirror and can be seen as an approximation of a parabola: $y^2 = 4fx$, where $f = r/2$. Since the parabola [6], brings all the incoming light to a single focus, the spherical mirror introduces an error Δx over a parabolic mirror:

$$\Delta x = \frac{y^4}{2^3 r^3} + \frac{y^6}{2^4 r^5} + \dots \tag{5}$$

Table 1

The errors Δx for a specific y and r (see also Fig. 4)

y (μm)	r (μm)	Absolute error Δx (μm)	Relative error $\Delta x/y$
2.25	3.0	0.2860	~ 10 %
1.50	3.0	0.0390	~ 20 %
0.75	1.5	0.0125	**~ 1.6 %**

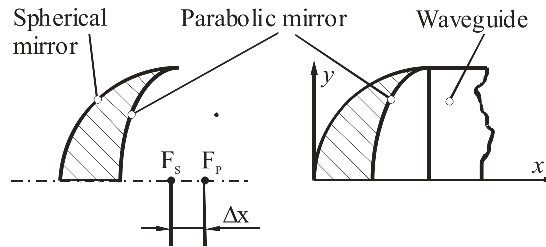

Fig. 4. Geometrical dimensions of the optical device showing the spherical aberration, Δx, between F_P (focus point of a parabolic mirror) and F_S (focus point of a spherical mirror).

4. Techniques for 3D structuring

Surfaces with well-defined dimensional shaping are required in several fields of microtechnology. Various techniques are used for 3D structuring, but all of them present some limitations. The main ones are the following.

- Anisotropic etching of silicon as the substrate material and the crystallographic orientation represent a restriction.
- The use of several masks for multiple etching or deposition steps (the limitations are due to alignment accuracy and the multiple steps). For example, using two masks, the desired profile can be approximated by four different depths.
- Variable-dose E-beam direct writing. Good results can be obtained using this method, which is particularly well suited for replication by embossing, but manufacturing costs are quite high.

- An alternative approach based on *gray-tone masks* (GTM) has been developed to generate 3D shapes, using conventional microelectronic equipment in only one exposure step.

Based on all above, we have selected the GTM method for our device fabrication.

The fabrication of 3D components using the GTM is done in three steps:

- the first –most critical step– concerns the realization of the GTM itself. This includes the definition of the zones of variable optical transmission inside 2D geometries that represent the various gray levels.
- in a second step, the wafers are exposed and the light intensity, modulated by the gray-tone areas on the mask, generates various depth in the photoresist.
- the profile in the photoresist is then proportionally transferred into the substrate during the third step.

During the design phase, gray levels are created by the repetition of dots that will appear as transparent holes in a chromium mask. These dots are small enough not to be transferred as such onto the wafer—because they are below the resolution limit of the exposure tool.

The dot matrices associated to the gray levels are then combined with the 2D geometries to define the final 3D structures.

Both, electron-beam and laser-beam pattern generators, have been tested at CSEM (Centre Suisse d'Electronique et de Microtechnique, Switzerland) for manufacturing GTM. The electron-beam pattern generator (EBPG-3) proved to be better suited for this application because of its flexibility and resolution.

The EBPG-3 has a minimum resolution of 25 nm and can be used for a finer final resolution. The exposure of the wafer can be realized using standard lithographic equipment, with a contact system. Slight modifications have been brought to the standard process, mainly by optimizing the exposure and the development parameters, in order to improve the profile and reach the correct depth. The desired continuous light intensity profile on a commercial Novolak-based positive photoresist was obtained by low-pass spatial filtering of the carrier pattern on the mask.

It has been practically proven that the resist profile is transferred into the appropriate substrate ($Si_xO_yN_z$) using plasma etching or ion milling technologies with controlled selectivity. Fig. 5 shows that the 3D profile is proportionally transferred from resist to fused silica.

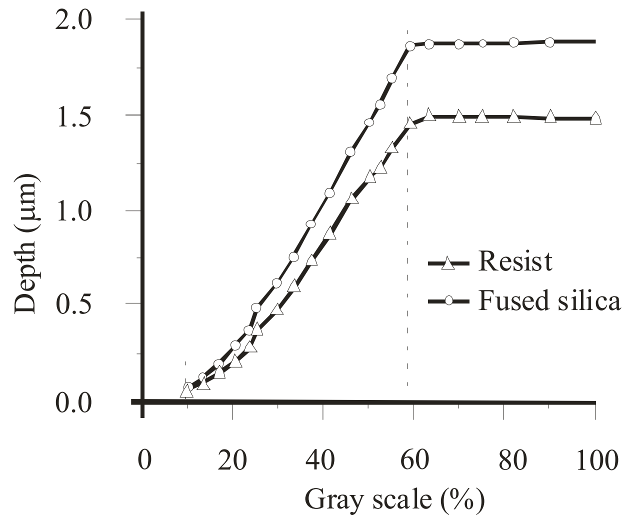

Fig. 5. Depth of test zones in resist, and in fused silica.
From http://farside.ph.utexas.edu/~rfitzp/teaching/302l/lectures/node114.htm

As can be seen from Fig. 5, there are three regions:

- a linear region from 10…60%;
- this is surrounded by two nonlinear regions: 0…10% and 60…100%.

This behavior reduces the number of gray tones from m to about $m/2$ as only about 50% of them can be transferred. Remark: these experimental curves have been used to generate the shades of gray of the final mask (see Appendix A) such as to obtain the desired 3D shape.

5. Mask design

The mask can be made on a chromium photoresist. During the etching process with an electron-beam installation, the spatial frequency (depending on how many gray–tone levels are) can be as low as 25 nm. This spatial frequency is given by the electron beam etching resolution and by the chromium GTM. The number of gray–tones m can be determined as:

$$m = w * 10^3 / 25 \qquad (6)$$

where 25 nm is the maximum resolution of the electron beam generator, and w is width of the device.

As can be seen from Table 2, when reducing the size of the device w, the number of gray tones m is also reduced, *limiting the applicability of this method to devices in the 1 μm range*.

Table 2

Number of gray tones (*m*) achievable for different device dimensions (*w*)

w [μm]	*m* [number of gray tones]
6.0	240
3.0	120
1.5	60
1.0	40
0.5	20

In the following we have chosen a depth of 1.5 μm that corresponds theoretically to 60 levels of gray. As explained before (see Fig. 5), only about 30 levels will be practically available. This number has been use as a parameter for the Matlab code which was written to automatically generate the colormap (see Appendix A).

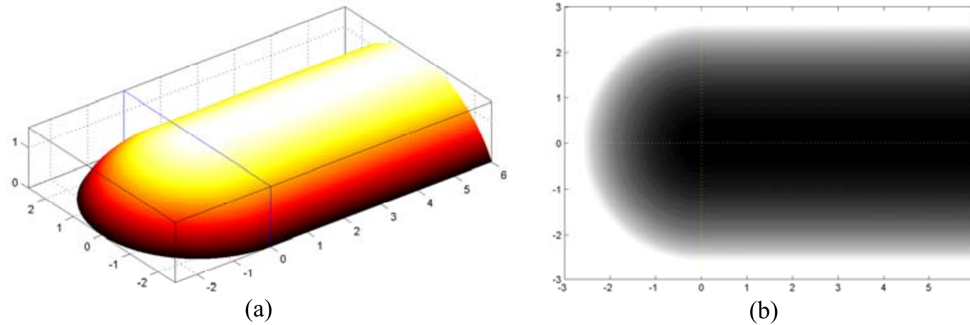

Fig. 6. a) 3D view of the optical fiber terminated with a spherical micromirror. The cross section of the fiber is a segment of a circle. b) The associated gray tone mask.

The first solution is using a spherical mirror, and can be seen in Fig. 6.a. Due to the spherical aberration, which is characteristic for such mirrors, we have decided to use only part of a sphere. The radius of the sphere is 3 μm, but the height of the micromirror is 1.5 μm. This height was imposed due to the technological constraints explained before. The cross section of the fiber has to match that of the micromirror, *i.e.*, a segment of a circle of height 1.5 μm.

The corresponding mask can be seen in Fig.6.b, with a colormap which has been generated based on the experimental curves discussed previously (see Fig. 5 and Appendices A, and B).

This solution has two disadvantages. The first one is represented by the fact that the mirror used has aberrations. This makes it that it will not be able to focus all the incoming light into one point. The shape of the cross section of the fiber is the second disadvantage. The fact that this is a segment of a circle, and

even more, a ‘thin’ one (height 1.5 μm, while the maximum width is about 6 μm), explains why light energy will be lost (due to a larger number of reflections).

The second solution is trying to improve on the previous one by enhancing both the shape of the micromirror as well as the cross section of the fiber. In this case the micromiror is a parabolic one [6] of height 1.5 μm. This will focus all the incoming light into one point, *if the rays are parallel to the principal axis*. The cross section is half a circle of radius 1.5 μm, coming closer to the ideal one: the full circle. The solution can be seen in Fig. 7 a (see also Appendix C).

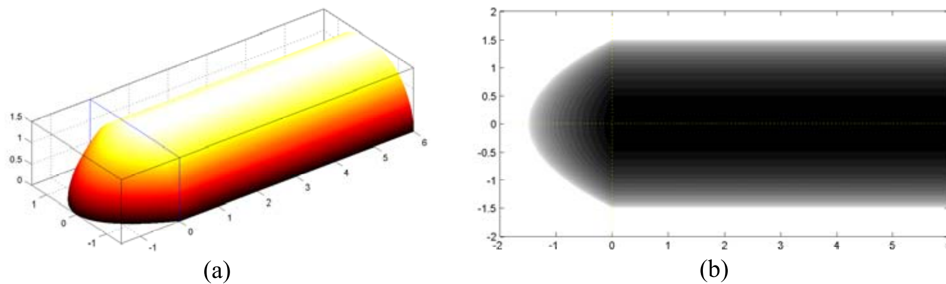

Fig. 7. a) 3D view of the optical fiber terminated with a parabolic micromirror. The cross section of the fiber is exactly half a circle. b) The associated gray tone mask.

Finally, the third solution is using a smaller section of a parabola, and corresponds to a rectangular cross section. The solution can be seen in Fig. 8.a.

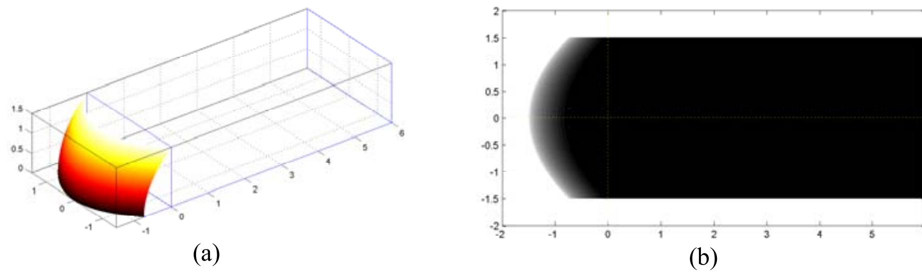

Fig. 8. a) 3D view of the optical fiber terminated with a parabolic micromirror. The cross section of the fiber is rectangular. b) The associated gray tone mask.

This is the best solution we have been able to come up with. The cross section is closer to a full circle than the previous two solutions. The smaller section of the parabola also makes it that the error for non-parallel incoming light rays will be smaller than in the previous two cases. The mask has been generated using the colormap presented before (Appendix A), and can be seen in Fig. 8.b (see also Appendix D). Obviously, this is significantly simpler than the previous

two masks, as most of it is of dark color (because no etching is required for generating a square cross section fiber).

6. Process flow

The core process is a classical CMOS n-well process (used for producing integrated circuits). The new devices (micromirror and wavegiude) can be integrated in this process in accordance with the following steps (see Fig. 9):

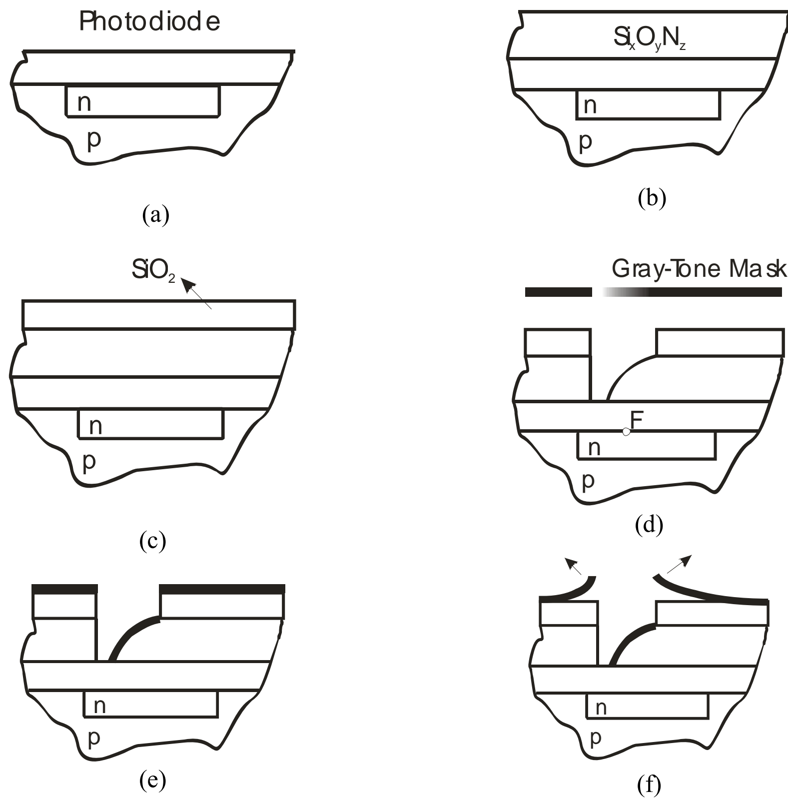

Fig. 9. The process flow for micromirror and fiber optics implementation: a) n-well implantation. b) Sputtering $Si_xO_yN_z$. c) Sputtering al SiO2 layer. d) Etching using a gray-tone mask. e) Sputtering thin film of Au [7, 8]. f) Lift-off technique for removing the undesired Au thin film

7. Conclusions

For a better understanding and an easier comparison of the three different solutions discussed, their 3D shapes have been overlapped and can be seen in Fig. 10.

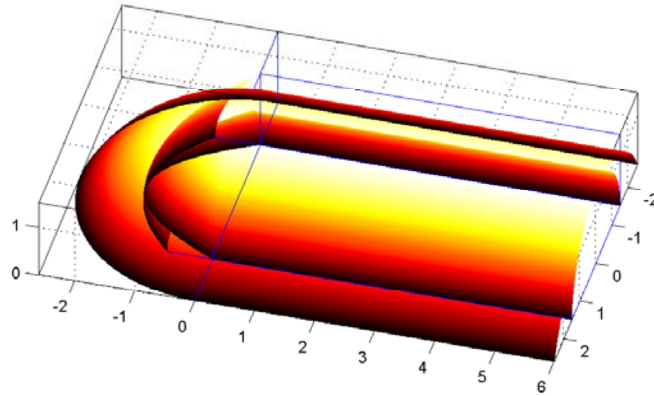

Fig. 10. 3D view of the three different solutions of terminating an optical fiber using a curved micromirror.

To conclude, we have theoretically investigated different ways of improving on the solution presented by Fullin *et al.* [3]. All these solutions are using fixed curved micromirrors.

Further work should be done for comparing the efficiency of these micromirrors when considered in conjunction with a certain cross section shape for the incoming fiber. These should be closely correlated with particular dimensions and material characteristics before building a test structure.

REFERENCES

[1]. *M.E. Motamedi, M.C. Wu, and K.S. Pister,* "Micro-opto-electromechanical devices and on-chip optical processing", in Optical. Eng., **vol. 36**, no. 5, May 1997, pp. 1282–1297.

[2]. *Y. Li, T. Wang, and K. Fasanella*, "Cost-effective side-coupling polymer fibre optics for optical interconnections," in J. Ligtwave Tech., **vol. 16**, no. 5, May 1998, pp. 892–901.

[3]. *L.Y. Lin, E.L. Goldstein, and R.W. Tkach*, "Free-space micromachined optical switches for optical networking," in IEEE J. Selected Topics Quantum Electr., **vol. 5**, no.1, Jan.-Feb. 1999, pp. 4–9.

[4]. *E. Fullin, G. Voirin, M. Chevroulet, A. Lagos, and J.-M. Moret*, "CMOS-based technology for integrated opto-electronics: A modular aproach", Electronic Dev. Meeting, Technical Digest, 11-14 Dec. 1994, pp. 527 –530.

[5]. *G.T.A. Kovacs*, Micromachined Transducers Sourcebook, Chapter 4.2. "Micromachined Reflective Components", McGraw-Hill, New York, 1998.

[6]. *J.W. Harris, and H. Stocker*, Handbook of Mathematics and Computational Science, Chapter 4.10.2 "Paraboloid of revolution", Springer-Verlag, New York, 1998.

[7]. *K. Cao, W. Liu, and J. J. Talgheder*, "Curvature compensation in micromirrors with high-reflectivity optical coatings," in J. of Microelectromechanical Sys., **vol. 10**, no. 3, Sep. 2001, pp. 409–417.

[8]. *U. Krishnamoorthy*, Design and fabrication of micromirrors for optical applications, Ph.D. Thesis, Univ. of California Davis, 2002. Accessible at http://www.stanford.edu/~ukris/.

Appendix

A.

```
max = 0.6;          % This corresponds to 60%
delta = 0.5;        % This represents the 'linear' region (60%-10%)
levels = 30;        % Half of the 60 levels achievable for 1.5 um
map(1,1) = max;
map(1,2) = max;
map(1,3) = max;
for i = 1:1:levels-1
    map(i+1,1) = max - delta*i/(levels-1);
    map(i+1,2) = max - delta*i/(levels-1);
    map(i+1,3) = max - delta*i/(levels-1);
end
colormap(map);
```

B.

```
rho = 3;            % Radius of 3 um
% Quarter of sphere
[theta, phi] = meshgrid(0:pi/180:pi/3, -pi/2:pi/180:pi/2);
z = rho*cos(theta);
x = rho*cos(phi).*sin(theta);
y = rho*sin(phi).*sin(theta);
surf(-x,-y,z-1.5);
shading('interp');
axis equal;
hold on;
% 6 um of fiber
[u, phi] = meshgrid(0:0.01:6, -pi/3:pi/180:pi/3);
v = rho*sin(phi);
w = rho*cos(phi);
surf(u,v,w-1.5);
shading('interp');
```

C.

```
a = 1.5;            % Parameter of the parabola 1.5 um
h = 1.5;            % Parameter of the parabola 1.5 um
step = 0.01;        % Precision for generating the mesh
% Half a parabola
[u, v] = meshgrid(0:step:a, -pi/2:pi/180:pi/2);
z = u;
x = a*sqrt(u/h).*cos(v);
y = a*sqrt(u/h).*sin(v);
surf(z-1.5,y,x);
shading('interp');
axis equal
hold on;
% 6 um of fiber
[u, phi] = meshgrid(0:0.01:6, -pi/2:pi/90:pi/2);
v = h*sin(phi);
w = h*cos(phi);
surf(u,v,w);
shading('interp');
```

D.

```
p = 1.5;            % Parameter of the parabola 1.5 um
step = 0.01;        % Precision for generating the mesh
% Section of a parabola
[x,y] = meshgrid(0:step:p, -p:step:p);
z = (x.*x+y.*y)/p/2;
surf(z-p,y,x);
shading('interp');
```